JOURNAL OF THERMOPHYSICS AND HEAT TRANSFER
Vol. 16, No. 3, July–September 2002

Heat Transfer in Two-Pass Turbulated Channels Connected by Holes

Srinath V. Ekkad,* David Kontrovitz,† Hasan Nasir,† Gautam Pamula,‡ and Sumanta Acharya§
Louisiana State University, Baton Rouge, Louisiana 70803

This is part of a continuing study of a new internal channel cooling design for modern gas-turbine blades. In previous studies, the enhanced cooling in the second pass of a serpentine channel was achieved by a combination of impingement and crossflow-induced swirl. A holed or slotted divider wall replaced the 180-deg U turn connecting the two legs of the serpentine channel. Flow from one coolant pass to the adjoining coolant pass was achieved through a series of straight and angled holes and a two-dimensional slot placed along the dividing wall. The focus is to enhance the heat transfer in the first pass of the two-pass channel using traditional rib turbulators. The effect of ribs in the first pass on the overall second pass heat transfer enhancement is compared to channels with no rib turbulators. Heat transfer distributions are compared for three channel flow Reynolds numbers ranging between 1.0×10^4 and 5.0×10^4. Three different rib configurations, 90-deg ribs, 60-deg angled forward facing toward the divider wall, and 60-deg angled backward facing away from divider wall, are studied for all Reynolds numbers and divider wall geometries. The presence of ribs in the first pass does not only decrease the enhanced heat transfer in the second pass, but also provides higher heat transfer enhancement in the first pass, resulting in an increase in overall heat transfer enhancement for the entire two-pass channel.

Nomenclature

b	=	divider wall thickness
D	=	square channel width or height
D_h	=	channel hydraulic diameter
d	=	hole diameter
f	=	Darcy friction factor, $2\Delta P(D_h/L)/(\rho \bar{V}^2)$
f_0	=	Darcy friction factor in all-smooth wall channel, $0.046Re^{-0.2}$
$\bar{\bar{f}}$	=	total channel averaged friction factor
h	=	convective heat transfer coefficient
k	=	thermal conductivity of test surface material
k_a	=	thermal conductivity of air
L	=	length of each pass
$\dot{m}$	=	mass-flow rate
Nu	=	Nusselt number, hD_h/k_a
Nu_0	=	fully developed flow Nusselt number, $0.023Re^{0.8}Pr^{0.4}$
$\bar{Nu}$	=	span averaged Nusselt number
$\bar{\bar{Nu}}$	=	area averaged Nusselt number
P	=	pressure
Pr	=	Prandtl number
p	=	hole spacing
Re	=	channel Reynolds number, $\rho \bar{V} D/\mu$
T	=	temperature
t	=	time of color change
$\bar{V}$	=	average flow velocity
X	=	axial distance from middle of turn
α	=	thermal diffusivity of test surface material
μ	=	dynamic viscosity of air
ρ	=	density

Subscripts

in	=	inlet condition
j	=	time step based
0	=	correlation based

Received 10 October 2001; revision received 14 January 2002; accepted for publication 15 January 2002.

*Assistant Professor, Mechanical Engineering Department; ekkad@me.lsu.edu. Member AIAA.
†Graduate Student, Mechanical Engineering Department.
‡Graduate Student, Mechanical Engineering Department; currently Consultant, Cap Gemini Ernst and Young LLC, 1221 Mckinney Street, Suite 2000, Houston, TX 77010.
§LR Daniel Professor, Mechanical Engineering Department. Member AIAA.

Introduction

THE present study focuses on new, improved internal channel designs for gas-turbine blades to provide higher heat transfer enhancement with relatively small changes to the airfoil internal cooling channel geometry. The conventional 180-deg U bend connecting the two passages is replaced with a channel divider wall that includes rows of cylindrical holes or slots that eliminate the 180-deg turn. The divider wall separates the two passes of the internal cooling scheme and normally acts as a conducting wall from the pressure to suction side of the airfoil. The cylindrical holes permit lateral injection from the first pass to the second pass. This leads to a combination of impingement and crossflow-induced swirl in the second pass that provides a higher overall heat transfer in the second passage. The first pass heat transfer can be enhanced with periodic rib turbulators without significantly affecting the swirl-induced high heat transfer coefficients in the second pass. This new cooling channel will help maintain blade temperatures at acceptable levels without using excessive coolant while providing longer life and durability. It is shown in this study that the pressure drop penalty to achieve high heat transfer coefficients is comparable to regular fully turbulated two-pass channels connected by 180-deg U turns.

Several researchers[1–4] presented enhanced heat transfer measurements in both the first pass and second pass using rib turbulators. The use of rib turbulators in the two-pass channel design increased both heat transfer enhancement and pressure drop. An optimal rib turbulator produces the highest heat transfer enhancement with minimal increase in pressure drop. Most of the researchers determined the 45–60-deg angled parallel rib provides the highest heat transfer enhancement and also a higher pressure drop than most rib configurations. Han and Zhang[5] also investigated several discrete rib configurations, broken and continuous, for heat transfer enhancement in straight square channels. Some of the configurations, although promising, present manufacturability problems and are not practical for usage.

Glezer et al.,[6] Ligrani et al.,[7] and Moon et al.[8] investigated the advantages of induced swirl in circular channels for heat transfer enhancement. They create swirl by injecting air into the tube through tangential slots along the wall. The importance of these studies is the indication that inducing swirl contributes to significantly higher heat transfer. Hedlund et al.[9] presented heat transfer measurements inside a circular swirl chamber for simulating turbine blade internal cooling. All of the aforementioned studies used circular channels.

This study is a continuation of the studies by Ekkad et al.[10] and Pamula et al.[11] Ekkad et al.[10] presented detailed heat transfer distributions in channels connected by one row of holes along the divider wall without a 180-deg turn. They varied the angle of the hole and also the location of the hole to determine the most effective geometry. They determined that the single-hole straight injection row design provides significant (up to 8–10 times) higher heat transfer coefficients than the 180-deg turn geometry. However, the pressure drop across the holes is also significant resulting in low thermal performance values around 1.2–2.0 thermal performance parameters given as $(\bar{N}u/Nu_0)/(\bar{f}/f_0)^{1/3}$. Although the inclined injection provided much higher heat transfer coefficients, the pressure drop was also significant, resulting in almost similar thermal performance numbers. Another important facet was the significantly different heat transfer distributions on the two sidewalls. Pamula et al.[11] studied the effect of two rows of holes on the divider wall compared to one row of holes in the case of Ekkad et al.[10] They created similar flow conditions along both sidewalls with similar hole configuration, feeding the coolant along the sidewalls. They determined that the increase in area of holes on the divider contributed to a significant drop in the heat transfer coefficients on the impingement wall, but increased heat transfer on the opposite sidewall due to dual injection or similar impingement. The pressure drop was also significantly lower for the two row cases and, thus, produced a similar or better overall thermal performance for the same Reynolds number condition compared to single-row cases. In both studies, the first pass acted more as a feeder channel and was not considered for heat transfer enhancement. In this study, the focus is on enhancing the heat transfer in the first pass in addition to the presence of the induced swirl and impingement in the second pass. It is necessary that the first pass heat transfer levels be similar to the second pass heat transfer levels to avoid thermal gradient-induced stresses by overcooling and undercooling in adjacent areas.

Experimental Setup

Figure 1 presents a schematic of the experimental setup. The experimental setup consists of an image processing system [red–green–blue (RGB) color charge-coupled device camera, 24-bit color frame grabber card, personal computer, and imaging software], temperature measurement system, flow loop, and the test section. The RGB camera is focused on the test section, and the color frame grabber card is programmed through the software to analyze real-time images for color signals during a transient heat transfer test. Details of the flow loop and test apparatus are provided by Ekkad et al.[10]

Figure 2a shows the schematic of the test channel with the new divider wall geometries. The various walls are identified in Fig. 2a. Case 1 refers to the two-pass channel with a 180-deg turn. Cases 2 and 3 represent the channels with two rows of holes in the divider wall along each sidewall. Case 4 is the channel with two-dimensional slots that vary in width from the middle of the channel to the endwall along the sidewalls. The sidewalls are the outer surfaces on both of the passages, orthogonal to the divider wall. The sidewalls are the primary heat transfer surfaces for which the results are presented. The outer walls of the test section are parallel to the divider wall. The wall of the test section that bounds the flow inside the passage where the flow is forced to enter the second passage is called the endwall.

The test channel is 5.08-cm square in cross section through the one-pass 60.96-cm length. The channel length to hydraulic diameter ratio (L/D_h) is 12. There is no 180-deg turn for the channels connected by the holes or slots. All of the flow goes through the holes or slots. The ratio of the total area of all of the holes/slots (cases 2–4) to the turn region area in the 180-deg-turn case was 1.2. The turn region is the area where there is no divider wall between the two passes. For the channels with holes, there are 24 holes of 1.27-cm diam with 12 holes in each row. Each hole row exit centerline is 1.27 cm from a sidewall. There are no holes along the divider wall for the first 30.48 cm of the channel length from entrance. The 12 holes in each row are then evenly distributed over the next 30.48 cm of the channel length. The holes are spaced two hole diameters

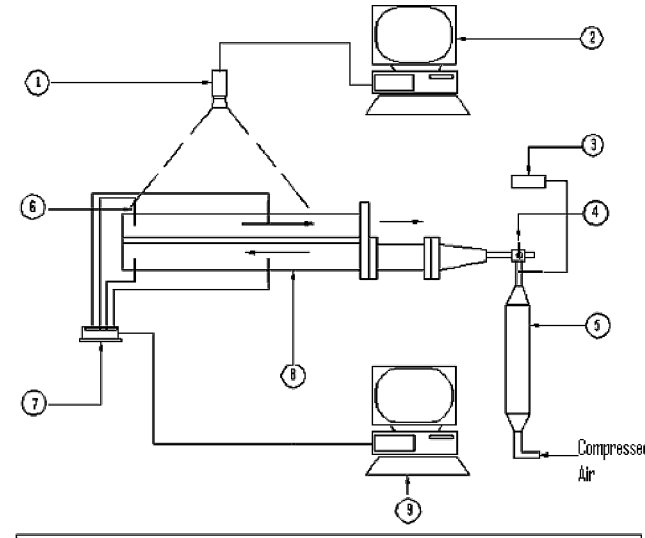

Fig. 1 Experimental setup.

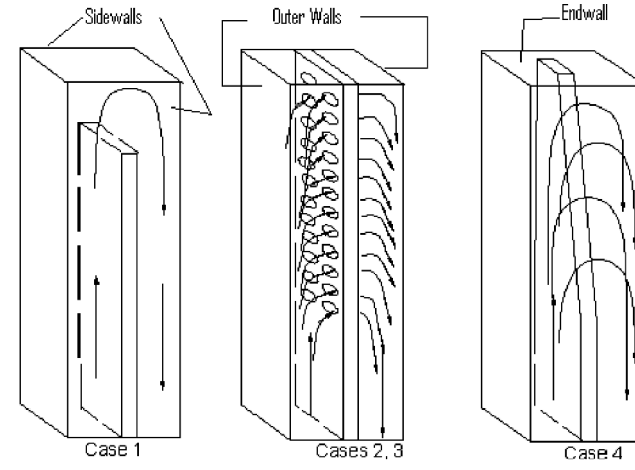

Fig. 2a Schematic of the two-pass channels.

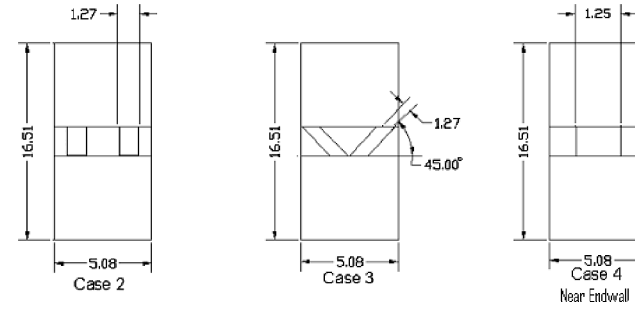

Fig. 2b Side view of the divider wall geometry for each case.

(centerline to centerline) apart. The hole locations on the divider wall were also designed to produce a swirling flow in the second pass. For the slotted divider wall, there are no slots for the first half of the channel length. The slots along the sidewalls increase in zero width at half-channel length to about 0.96-cm width at the endwall. The slots are identical along both sidewalls, resulting in similar flow distributions along both sidewalls (1.27 cm thick). Pamula et al.[11] provide more details on the divider wall geometry.

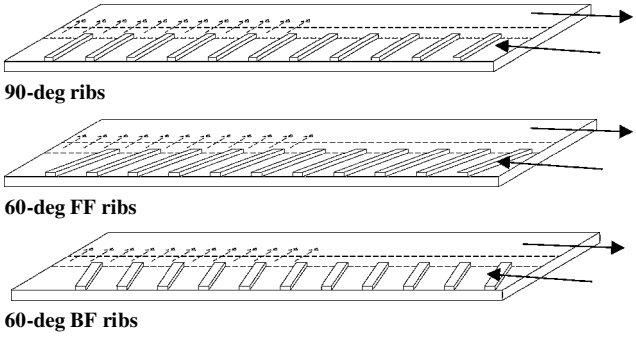

Fig. 3 Schematic of the rib arrangement on each sidewall.

Figure 2b shows the channel geometries studied. Case 2 shows the straight injection configuration. Case 3 shows the inclined hole geometry. The holes are inclined at 45 deg to the vertical direction. Case 4 shows the slot geometry. The two-dimensional slots were chosen instead of a uniform slot width to create more uniform flow through the slot, from the beginning of the slot to the endwall.

Figure 3 presents the rib turbulator configurations studied. Ribs are placed along both of the sidewalls at the same axial location, only in the first pass. Three different rib configurations have been compared to the no-rib geometry studied by Pamula et al.[11] The three rib configurations are 1) 90-deg parallel, 2) 60-deg forward facing (60-deg FF), and 3) 60-deg backward facing (60-deg BF). The 90-deg ribs are orthogonal to the first-pass flow in the streamwise direction. The 60-deg FF ribs are directed from the outer wall toward the divider wall at an angle of 60 deg to the flow, and the 60-deg BF ribs are directed away from the divider wall toward the outer wall at an angle of 60 deg to the flow. The ribs are placed on both sidewalls at the same axial location. This arrangement is typically called in-line configuration. The ribs were made of light balsa wood, and so they do not absorb heat and maintain the one dimensionality of the wall. In the real engine, both the channel walls and the ribs are of the same material because they are cast as one piece.

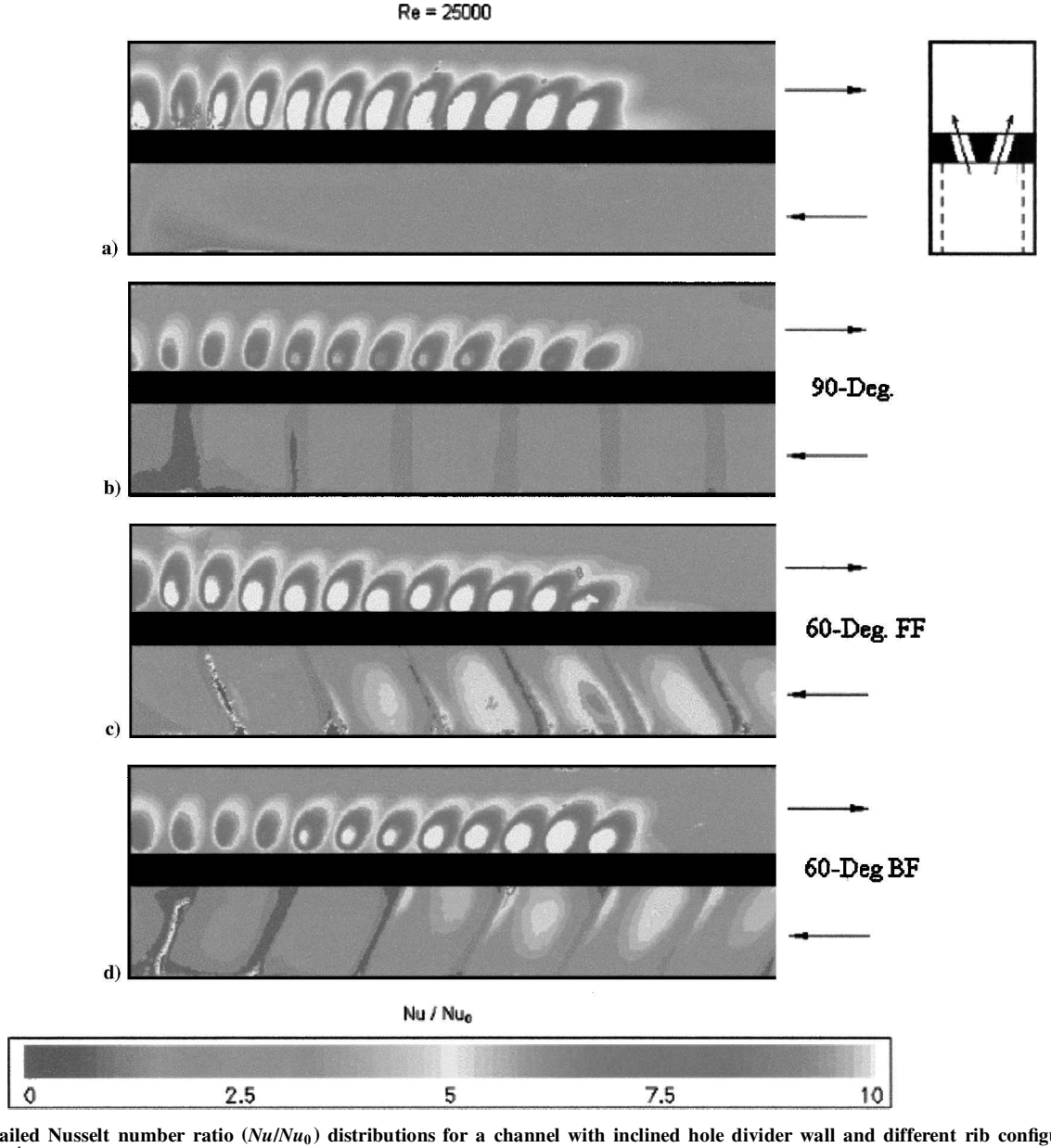

Fig. 4 Detailed Nusselt number ratio (Nu/Nu_0) distributions for a channel with inclined hole divider wall and different rib configurations at $Re = 2.5 \times 10^4$.

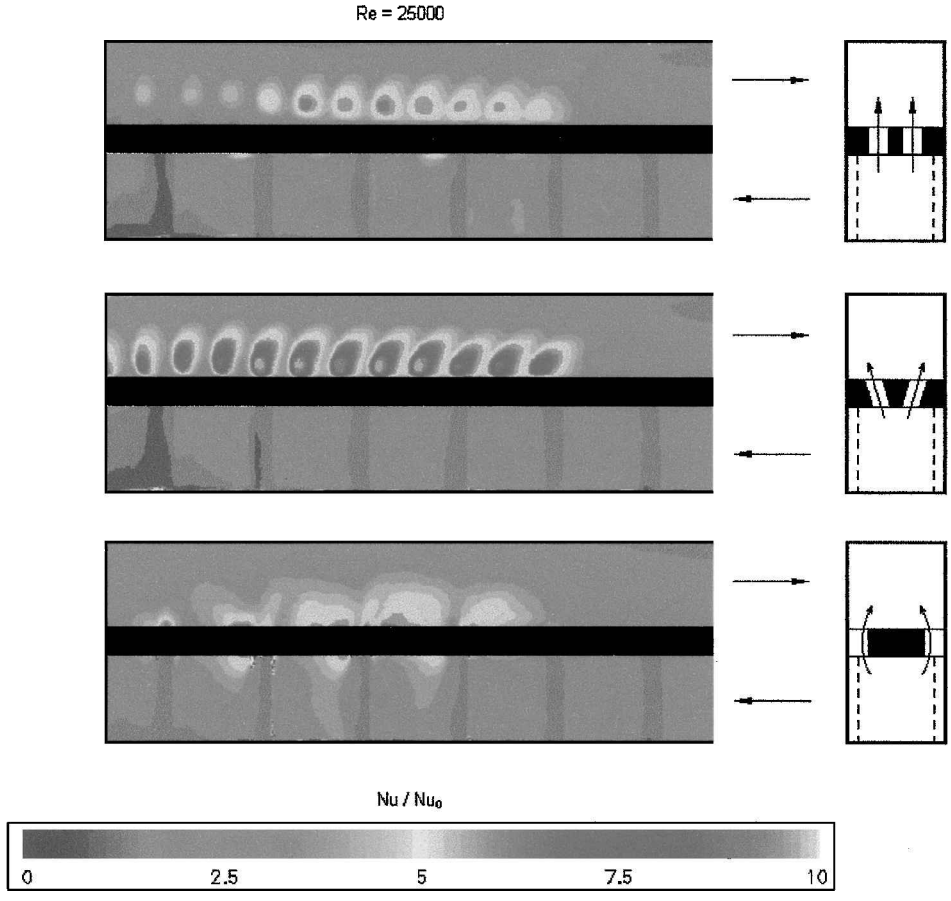

Fig. 5 Detailed Nusselt number ratio (Nu/Nu_0) distributions for a channel with 90-deg ribs with different divider wall geometry at $Re = 2.5 \times 10^4$.

The heat transfer measurements are made only on one of the sidewalls of the plexiglass test section. The surface is coated on the inside with a thin layer of thermochromic liquid crystals. A black paint coating is sprayed over the liquid crystal coating to ensure visibility of the liquid crystal color changes when viewed from the outside. Once the test section is coated with both the liquid crystal and black paint layers, the sidewalls of the channel are opaque. Thermocouples are placed at inlet and outlets of each passage (a total of four) to measure the local temperatures of the heated air. The transient thermocouple outputs are digitized during the test using an eight-channel A/D system.

Procedure and Data Reduction

The test procedure is exactly the same as used in the earlier studies.[10,11] The liquid crystal coating used in this study has a narrow band with the initial red color appearing at 35.1°C, then green color appearance at 35.4°C, and finally blue color at 35.9°C. The total band is 1°C. The region of interest was divided into 500 × 200 pixels. The reference point is set at the appearance of green color during the transient test. The test duration is typically a maximum of 150 s.

The test section is made of plexiglass so that a one-dimensional semi-infinite solid assumption can be applied on the test section wall.[3,12] The local air bulk temperature for each axial pixel location is interpolated from the measured thermocouple locations. The time-step changes are then included into the equation[3,12] to obtain a function of the form

$$T_w - T_i = \sum_{j=1}^{N} \left\{ 1 - \exp\left[\frac{h^2 \alpha (t - \tau_j)}{k^2} \right] \times \operatorname{erfc}\left[\frac{h\sqrt{\alpha (t - \tau_j)}}{k} \right] \right\} \left[\Delta T_{m,(j,j-1)} \right]$$

where $\Delta T_{m,(j,j-1)}$ and τ_j are the mainstream temperature and time step changes for the integration scheme interpolated from the digitized temperature outputs. The equation is solved at every pixel location to obtain the local heat transfer coefficient h.

The total pressure drop ΔP across the channel is measured, and the Darcy friction factor, $2\Delta P(D_h/L)/(\rho \bar{V}^2)$, is determined for each flow condition for each geometry. The friction factor is normalized using the smooth tube flow friction factor f_0, calculated using $0.046Re^{-0.2}$.

The average experimental uncertainty in the heat transfer coefficient measurements, based on the methodology of Kline and McClintock,[13] is on the order of ±7.4%. The uncertainty in friction factor measurement is on the order of ±8.0%. Details on the uncertainty analysis are presented by Ekkad et al.[10]

Results and Discussion

The measured heat transfer coefficients are presented in the form of Nusselt numbers based on channel inlet hydraulic diameter ($Nu = hD_h/k_a$). The local Nusselt numbers are then normalized by the Nusselt number using the channel inlet Reynolds number for a fully developed pipe flow condition using the Dittus–Boelter correlation ($Nu_0 = 0.023Re^{0.8}Pr^{0.4}$). The results presented in this study are higher than the Dittus–Boelter equation for the no-rib cases because the flow is not fully developed when it is exposed to the first hole in the divider wall. However, all of the results are consistently normalized by the same number. All of the results are presented as normalized Nusselt numbers in this paper. The heat transfer distributions at the rib locations are incorrect because the technique measures the heat transfer coefficient underneath nonconducting ribs and shows very low values. The heat transfer coefficients on top of the ribs are much higher than the surface wall, as shown by Ekkad and Han.[3] In this study, the on-rib heat transfer coefficients are not measured and, thus, not considered in the averaging process. Typically, the on-rib heat transfer coefficients are very high, as shown by

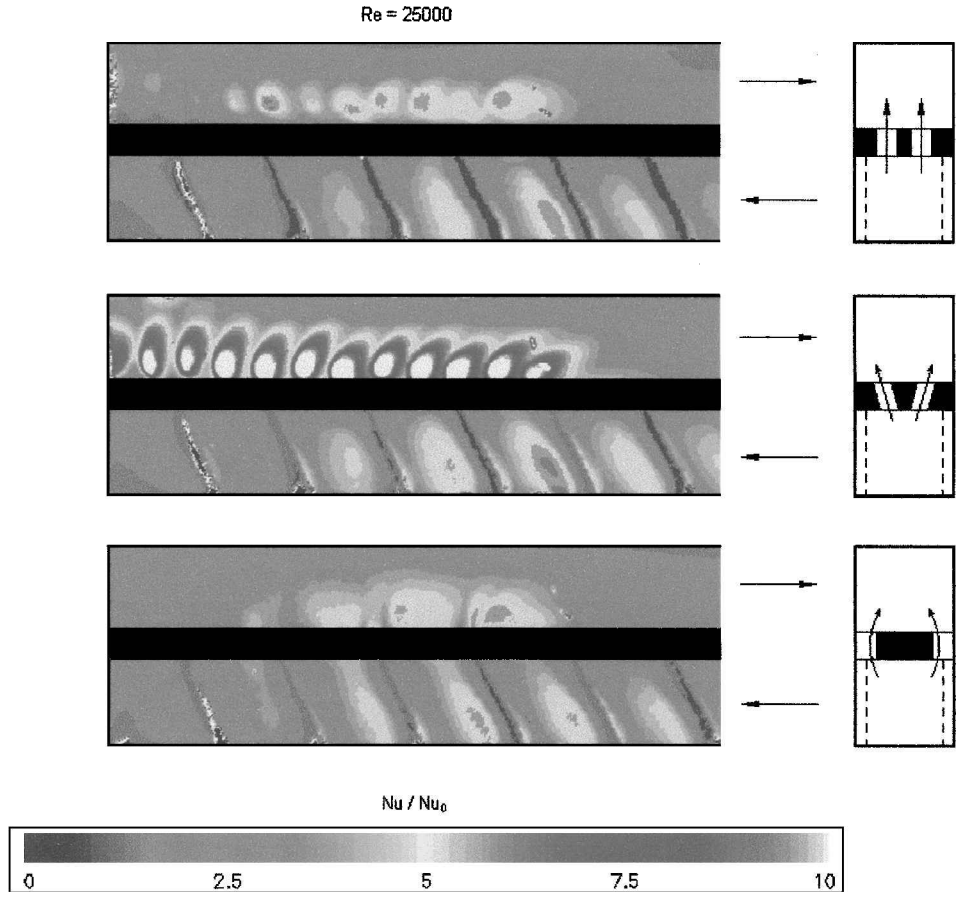

Fig. 6 Detailed Nusselt number ratio (Nu/Nu_0) distributions for a channel with 60-deg FF ribs with different divider wall geometry at $Re = 2.5 \times 10^4$.

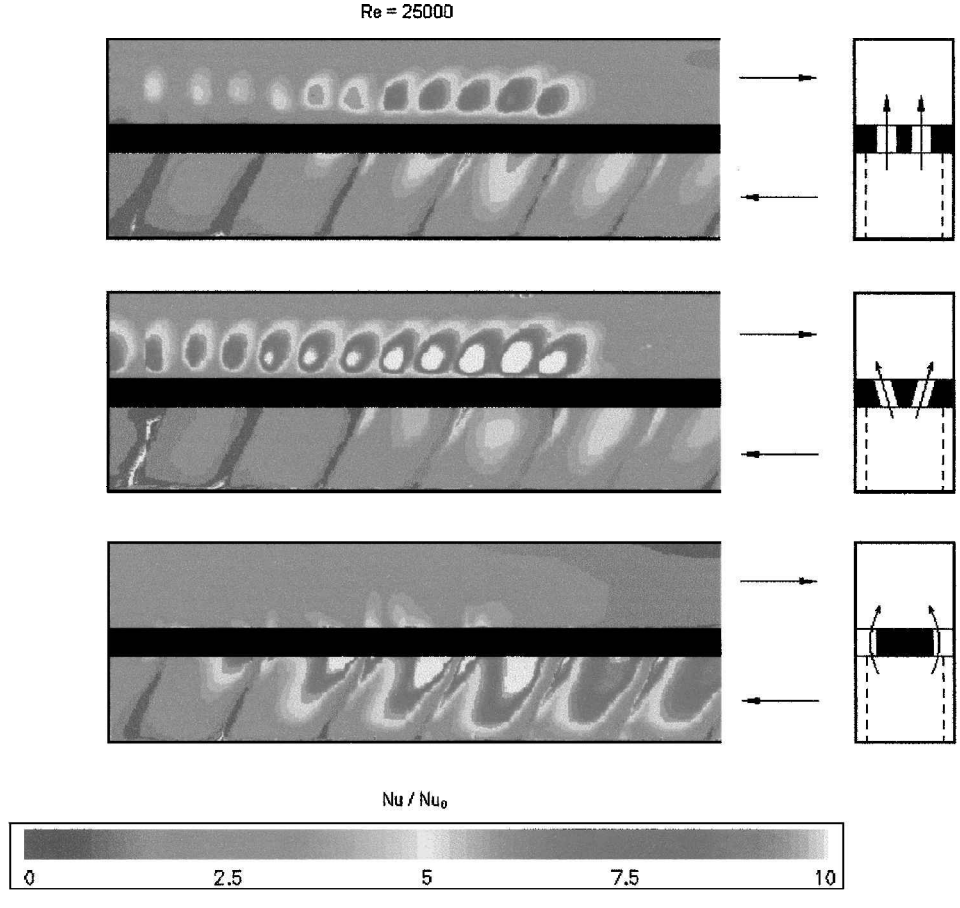

Fig. 7 Detailed Nusselt number ratio (Nu/Nu_0) distributions for a channel with 60-deg BF ribs with different divider wall geometry at $Re = 2.5 \times 10^4$.

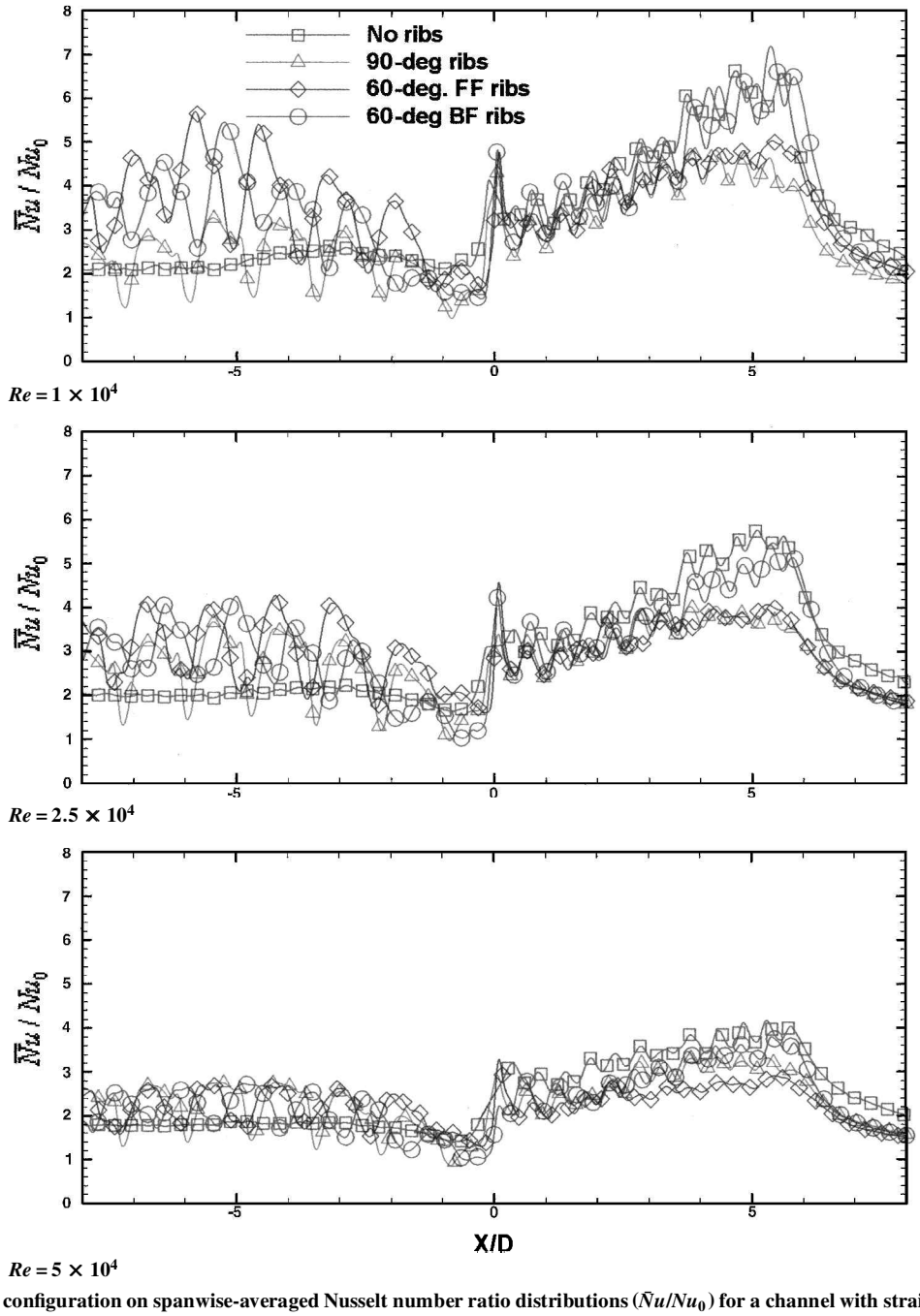

Fig. 8 Effect of rib configuration on spanwise-averaged Nusselt number ratio distributions ($\bar{N}u/Nu_0$) for a channel with straight hole divider wall.

Ekkad and Han.[3] Results are presented for only one sidewall because the opposite sidewall has similar heat transfer distributions due to the geometrical symmetry along the channel centerline through the middle of the divider wall.

Figure 4 presents the detailed Nusselt number ratio distributions for case 3 on one sidewall with different rib configurations at $Re = 2.5 \times 10^4$. Figure 4a presents the no-rib case from Pamula et al.[11] The local high regions in the second pass are where the impingement occurs from the flow through the holes from the first pass. The Nusselt number ratios are higher than 10 inside the impingement core regions. As the flow moves downstream toward the exit in the second pass, the jet impingement location is pushed streamwise to the divider wall. The impingement effect decreases toward the endwall due to the decreased pressure difference across the holes and the resulting reduced flow rates.[11] The maximum Nusselt number ratio in the core impingement region are on the order of 12–13. Figure 4b shows the effect of turbulating the first pass with 90-deg orthogonal ribs. The first-pass distributions are typical of rib turbulated channels with periodic high and low regions where flow separates and reattaches. Reliable data are not available on top of the ribs. Enhancement levels are around 2.0–3.0 between the ribs. In the second pass, the ribs appear to have caused a significant reduction in Nusselt number ratios. This may be due to the increased pressure drop in the channel and the flow distributions in the first pass due to the presence of the ribs at the same Reynolds number. The Nusselt number ratios inside the impingement core regions are reduced to around 8.0. Figure 4c shows the channel with 60-deg FF ribs. The heat transfer enhancement in the first pass is higher, as should be expected for 60-deg ribs over 90-deg ribs. However, note that the second-pass heat transfer ratios are affected only slightly due to the presence of the ribs as compared to the results in Fig. 4a. The ribs are angled toward the divider wall, and it is believed the secondary flows generated by the ribs from the outer wall to the divider wall push the flow toward the holes, creating reduced pressure

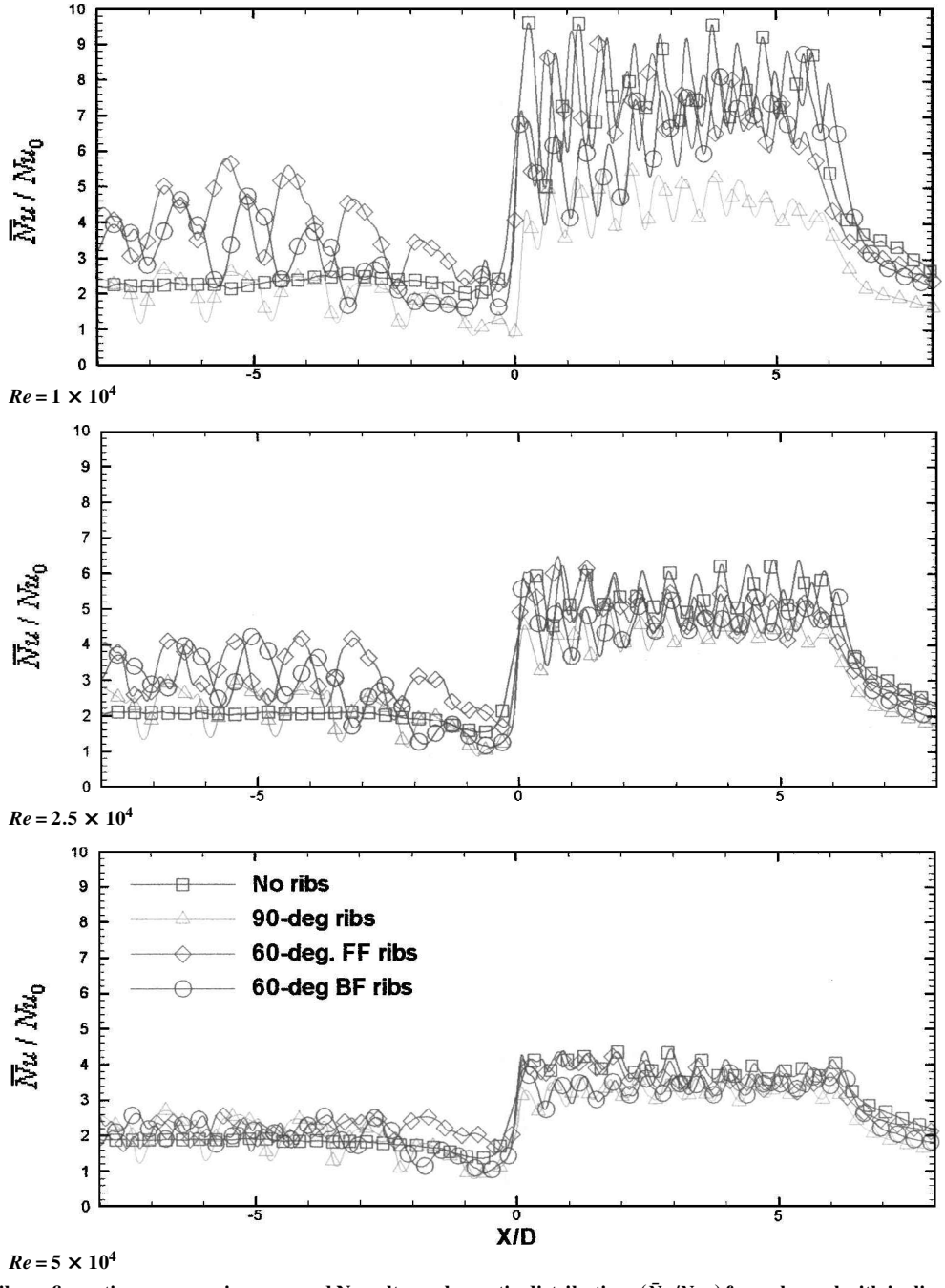

Fig. 9 Effect of rib configuration on spanwise-averaged Nusselt number ratio distributions ($\bar{N}u/Nu_0$) for a channel with inclined hole divider wall.

drop and increasing jet velocities coming out of the holes. Also, because the secondary flow structures are generated at the rib starting point away from the divider wall, the heat transfer enhancement is higher in that region.[3] Figure 4d shows the channel with 60-deg BF ribs. The ribs enhance heat transfer in the first pass, similar to that for 60-deg FF ribs. However, the second-pass enhancements are lower near the endwall far from the exit. The secondary flow direction for these ribs is from the divider wall toward the outer wall. This direction is opposite to the main flow direction. The driving pressure difference for the flow is across the holes. The secondary flows impede the main flow through the holes and, thus, increase the pressure drops and, thus, produce reduced jet impingement and lower Nusselt number ratios. This effect is more prominent for the jet holes closer to the endwall.

Figure 5 presents the effect of divider wall geometry for a channel with 90-deg rib turbulators for $Re = 2.5 \times 10^4$. The detailed Nusselt number ratios clearly show that the inclined hole geometry performs the best for heat transfer enhancement in the second pass. However, the tapered slot enhances the heat transfer highest in the first pass. Because the slot is continuous along the divider wall, the airflow migrates toward the slots and creates a sheet flow effect that increases the heat transfer in regions where the flow velocity is higher. This is at the sidewall where the slot width is near zero to moderate widths.

Figure 6 presents the effect of divider wall geometry for a channel with 60-deg FF rib turbulators for $Re = 2.5 \times 10^4$. For this configuration also, the inclined hole geometry performs significantly better in the second pass than the other two wall geometries. The first pass enhancement is similar for all three cases.

Figure 7 presents the effect of divider wall geometry for a channel with 60-deg BF rib turbulators for $Re = 2.5 \times 10^4$. For this configuration also, the inclined hole geometry provides very high Nusselt

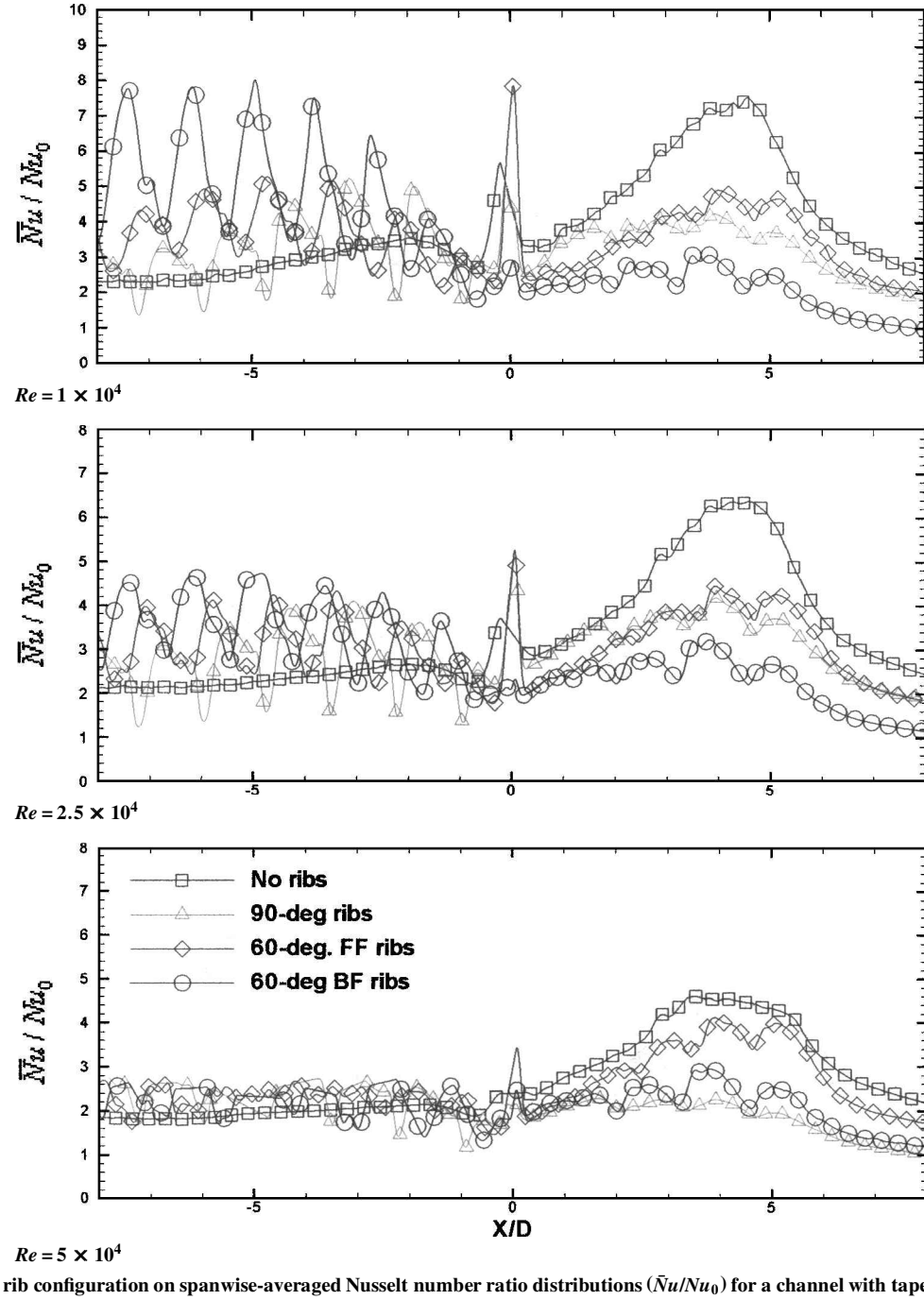

Fig. 10 Effect of rib configuration on spanwise-averaged Nusselt number ratio distributions ($\bar{N}u/Nu_0$) for a channel with tapered slot divider wall.

number ratios in the second pass. The second-pass enhancement with the tapered slot geometry is significantly lower. This may be due to the rib-created secondary flow away from the divider wall. In the first pass, the tapered slot geometry provides significantly higher Nusselt number ratios than the other two cases. This may be due to the strong secondary flow induction along the rib angle and the associated slot width-induced flow rates.

All of the detailed distributions are presented for $Re = 2.5 \times 10^4$. Discussion about the results for other Reynolds number are presented as a comparison to the results presented for $Re = 2.5 \times 10^4$ in Figs. 8–13.

Figure 8 presents the effect of rib configuration on spanwise-averaged Nusselt number ratios ($\bar{N}u/Nu_0$) vs streamwise location for a channel divider wall with straight holes (case 2). In the first pass, all of the rib configurations provide higher heat transfer enhancement than the no-ribs case. The 60-deg rib cases provide higher enhancement than the 90-deg ribs as expected. This is consistent with the results presented by many studies on rib-enhanced heat transfer. In the second pass, the no-ribs channel provides the highest enhancement. The 60-deg BF rib configuration provides similar levels of enhancement as those for the no-ribs case. The other two rib cases also provide high enhancement but are lower than the no-ribs case. This indicates that a 90- or 60-deg FF rib configuration affects the jet impingement-induced heat transfer enhancement in the second pass as reported by Pamula et al.[11] for the no-rib channels. For a divider wall with straight hole geometry, a 60-deg BF rib configuration provides the best results. With an increase in Reynolds number from 1×10^4 to 5×10^4, the effect of rib and rib configuration decreases. It appears that, at higher Reynolds number, the effect of the rib is seen only in the first pass, providing enhancements of up to 2.0 over the no-rib channel. The results in the second pass show lesser divergence from the no-ribs channel case.

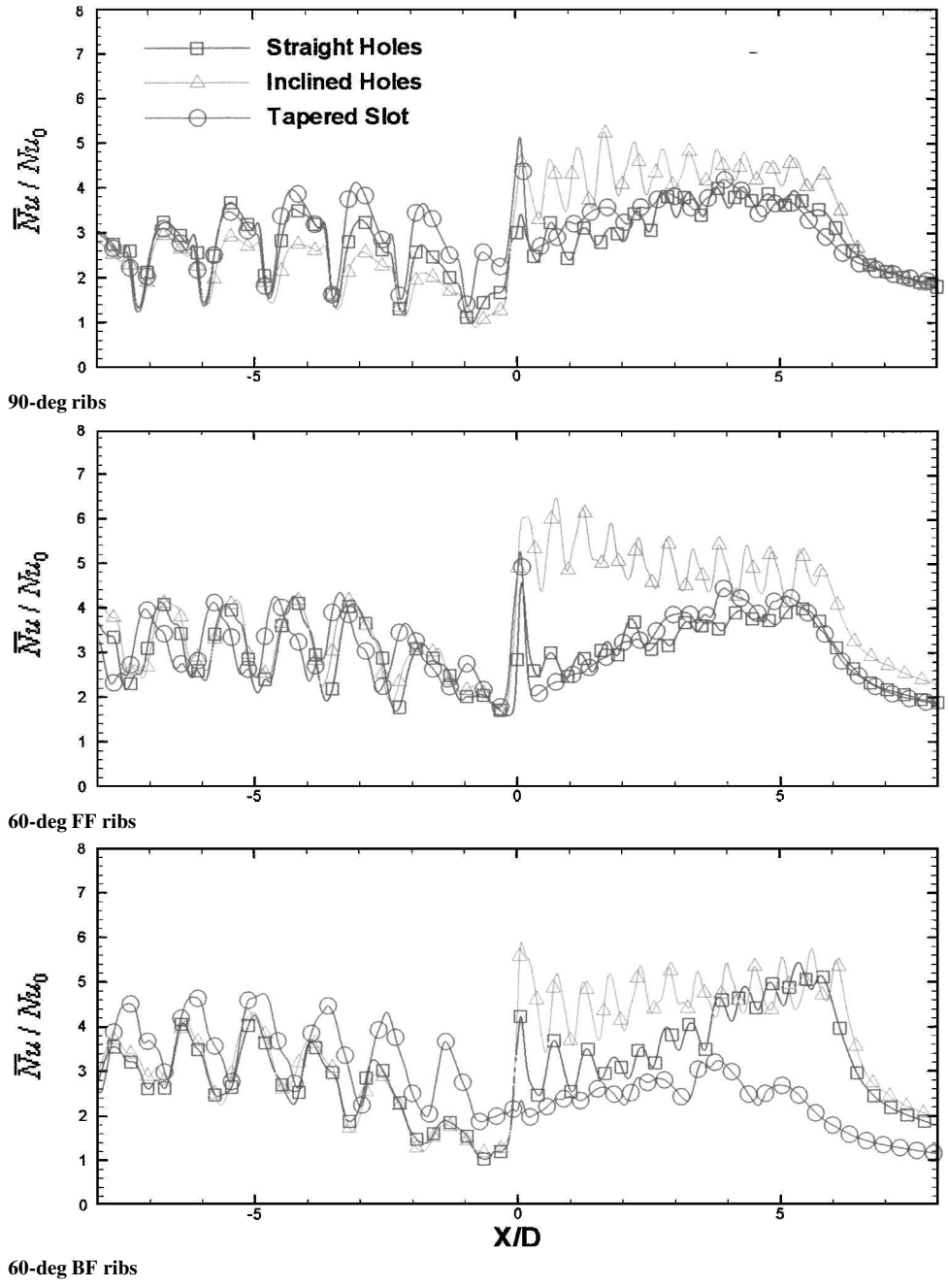

Fig. 11 Effect of divider wall configuration on spanwise-averaged Nusselt number ratio distributions ($\bar{N}u/Nu_0$) for channels with different rib configurations.

Figure 9 presents the effect of rib configuration on spanwise-averaged Nusselt number ratios ($\bar{N}u/Nu_0$) for a channel divider wall with inclined holes (case 3). Results show that the ribs enhance the heat transfer in the first pass significantly at low Reynolds numbers. The second pass heat transfer enhancement is unaffected by the ribs, except for the case of 90-deg ribs. With further increase in Reynolds number, the effect of rib configuration and the presence of ribs is not significant as compared to the no-rib case. Heat transfer enhancement in the first pass levels to about 1.5 to 2.0 times the no-rib case and the second pass enhancement is similar for all cases except as noted for 90-deg ribs at low Reynolds number.

Figure 10 presents the effect of rib configuration on spanwise-averaged Nusselt number ratios ($\bar{N}u/Nu_0$) for a channel divider wall with tapered slot (case 4). The effect of ribs in the first pass is similar in this case to the other cases. However, at low $Re = 1 \times 10^4$, the 60-deg BF rib produces significant enhancement over the other rib configurations and the no-rib case. In the second pass, the presence of the rib considerably reduces the heat transfer enhancement produced by the swirl behavior through the slots. The 60-deg BF rib produces significantly lower Nusselt number ratios in the second pass. The other two rib configurations produce higher Nusselt number ratios than the 60-deg BF rib, but lower than the no-rib case. The effect is reduced with increasing Reynolds numbers. In all, the tapered slot with 60-deg BF ribs produces detrimental results compared to the no-ribs case. Results inside the slot region where there is no divider wall were not obtained because of the opacity of the outside wall.

Figure 11 presents the effect of channel divider wall geometry on spanwise-averaged Nusselt number ratios ($\bar{N}u/Nu_0$) for different rib configurations at $Re = 2.5 \times 10^4$. For the 90-deg ribs, the first pass is unaffected by the divider wall geometry. In the second pass, the inclined holes produce the highest heat transfer enhancement.

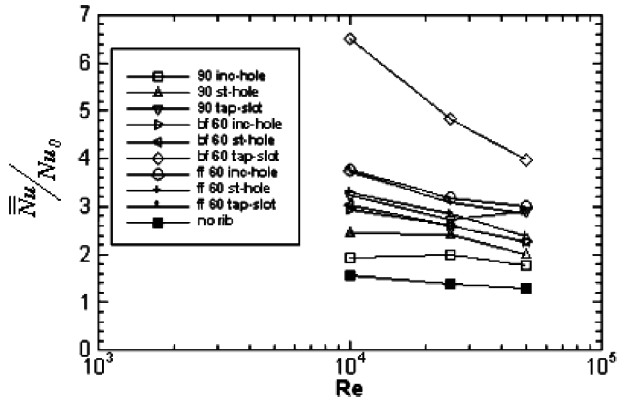

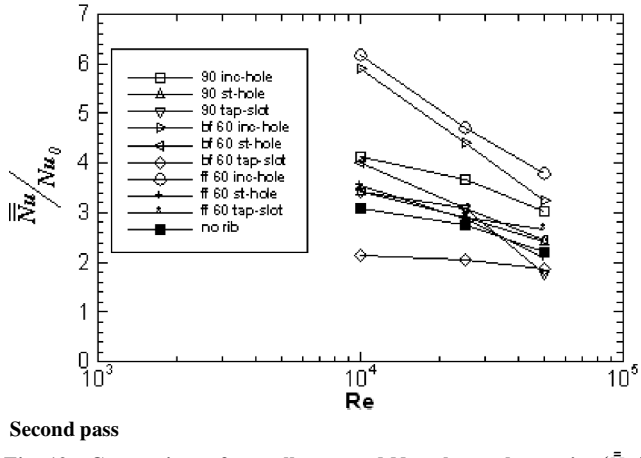

Fig. 12 Comparison of overall averaged Nusselt number ratios ($\bar{\bar{N}}u/Nu_0$) for different configurations vs Reynolds numbers.

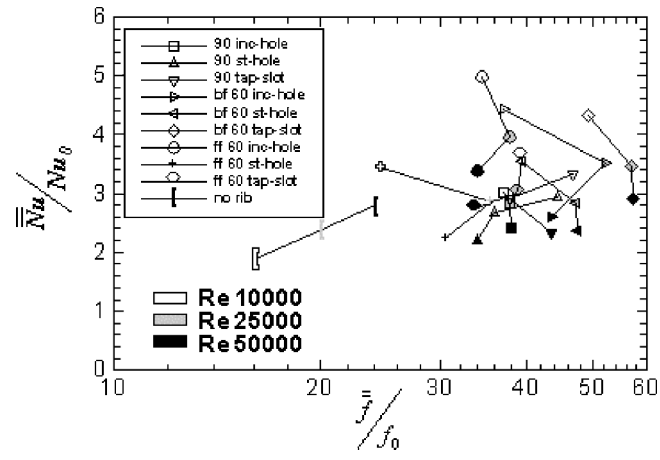

Fig. 13 Comparison of overall averaged Nusselt number ratios ($\bar{\bar{N}}u/Nu_0$) vs overall friction factor enhancement ($\bar{\bar{f}}/f_0$) for different configurations.

This is consistent with the results for the no-ribs case shown by Pamula et al.[11] The straight holes and the tapered slot produce similar levels of enhancement. For the 60-deg FF ribs, the first pass is again unaffected by the divider wall geometry. In the second pass, the inclined holes produce significantly higher Nusselt number ratios than the other two cases. For the 60-deg BF ribs, the tapered slot wall produces higher Nusselt number ratios in the first pass compared to the other two cases. However, in the second pass, the inclined holes produce the highest enhancement. The tapered slot produces lower heat transfer enhancement in the second pass compared to the first pass results.

Figure 12 presents the overall averaged Nusselt number ratios ($\bar{\bar{N}}u/Nu_0$) for the first pass and second pass vs flow Reynolds number. The symbols are labeled as the rib type and the divider wall case for each case. The tapered slot with 60-deg BF ribs provides the highest heat transfer enhancement in the first pass. The inclined hole geometry with 90-deg ribs provides the lowest enhancement. All of the other cases provide enhancement ratios in the range from 2.5 to 3.5. In the second pass, the inclined hole geometry with 60-deg FF ribs provides the highest 14 enhancement. The tapered slot with 90-deg ribs also provides similar high heat transfer enhancements. The tapered slot with 60-deg BF ribs has the lowest enhancement in the second pass. This was the case that provided the highest enhancement in the first pass. The other cases provide enhancement ratios in the range 2.5–4.0 for the second pass. Note that inclined holes with 60-deg FF ribs have the highest heat transfer enhancement in the second pass and the second highest in the first pass, indicating that this configuration may be the best overall performer among all of the cases tested. The baseline case for the whole study is the 180-deg turn channel without ribs. This is also included in Figs. 8–10 as the no-ribs case. The results show as expected for the first pass, with the 180-deg turn channel having the lowest ratios. The second pass shows some interesting results in that the 180-deg turn without ribs is higher than the 60-deg BF slot configuration.

Figure 13 presents the overall heat transfer enhancement for both passages combined as a function of the friction factor enhancement over the entire channel ($\bar{\bar{f}}/f_0$). The friction factor is calculated using the measured overall pressure across the entire channel. The optimum configuration for heat transfer enhancement will show higher heat transfer enhancement for a relatively lower friction factor enhancement. This indicates that the configuration for heat transfer enhancement is beneficial, regardless of the increased pressure drop over the entire channel. Figure 13 clearly shows that the inclined hole geometry with 60-deg FF ribs is the optimum configuration. Some of the other cases provide lower friction factor enhancement, but also provide lower heat transfer enhancement. Still other cases that provide similar heat transfer enhancement also show a significant rise in friction factor. The baseline case (180-deg turn, no ribs) is also shown for comparison. The overall heat transfer enhancement is lowest for this case and the friction factors are also the lowest.

Conclusions

Detailed heat transfer distributions are presented for two-pass channels connected by holes/slots in the divider wall with rib turbulators in the first pass. The overall enhancement obtained for this new internal cooling design is significant. Three configurations of holes/slots have been tested for a range of Reynolds numbers (1.0×10^4–5.0×10^4). The divider wall with inclined holes provides the highest heat transfer enhancement without ribs. It also produces the higher pressure drops compared to the other two divider wall geometries. Three rib configurations are tested with each of the divider wall geometries at all flow Reynolds numbers. The tapered slot wall with 60-deg BF ribs provided the highest heat transfer enhancement in the first pass and the inclined holes wall with 60-deg FF ribs provided the highest heat transfer enhancement in the second pass. The inclined holes wall with 60-deg FF ribs provided the highest overall heat transfer enhancement for the combined two-pass channel. This configuration is the best among the tested geometries because the associated pressure drop, presented as friction factor enhancement, is relatively lower for this case.

This design may eliminate the need for ribs in the second pass due to the significantly high heat transfer enhancement achieved. The overall pressure drop or friction factor is lower for this design than the traditional serpentine channel with 60-deg ribs. There are not much archival data on the pressure drop for two-pass channels connected by a 180-deg U bend with rib turbulators. The heat transfer enhancement levels are significantly higher for the proposed geometry compared to a two-pass channel with 180-deg bend and ribs.

Acknowledgments

The authors wish to acknowledge the support from the project funded by Louisiana Board of Regents through the NASA–LaSPACE REA under Contract NASA/LEQSF (1996–2001). The Program Manager is John Wefel.

References

[1]Han, J. C., "Heat Transfer and Friction Characteristics in Rectangular Channels with Rib Turbulators," *Journal of Heat Transfer*, Vol. 110, No. 3, 1988, pp. 321–328.

[2]Chandra, P. R., Han, J. C., and Lau, S. C., "Effect of Rib Angle on Local Heat/Mass Transfer Distribution in a Two-Pass Rib-Roughened Channel," *Journal of Turbomachinery*, Vol. 110, No. 1, 1988, pp. 70–79.

[3]Ekkad, S. V., and Han, J. C., "Detailed Heat Transfer Distributions in Two-Pass Square Channels with Rib Turbulators," *International Journal of Heat and Mass Transfer*, Vol. 40, No. 11, 1997, pp. 2525–2537.

[4]Hibbs, R., Acharya, S., Chen, Y., Nikitopoulos, D., and Myrum, T., "Heat Transfer in a Two-Pass Internally Ribbed Turbine Blade Coolant Channel with Cylindrical Vortex Generators," *Journal of Turbomachinery*, Vol. 120, No. 4, 1998, pp. 724–734.

[5]Han, J. C., and Zhang, Y. M., "High Performance Heat Transfer Ducts with Parallel, Broken, and V-Shaped Ribs," *International Journal of Heat and Mass Transfer*, Vol. 35, 1992, pp. 513–523.

[6]Glezer, B., Moon, H. K., and O'Connell, T., "A Novel Technique for the Internal Blade Cooling," American Society of Mechanical Engineers, ASME Paper 96-GT-181, June 1996.

[7]Ligrani, P. M., Hedlund, C. R., Thambu, R., Babinchak, B. T., Moon, H. K., and Glezer, B., "Flow Phenomena in Swirl Chambers," American Society of Mechanical Engineers, ASME Paper 97-GT-530, June 1997.

[8]Moon, H. K., O'Connell, T., and Glezer, B., "Heat Transfer Enhancement in a Circular Channel Using Lengthwise Continuous Tangential Injection," International Heat Transfer Conf., Aug. 1998.

[9]Hedlund, C. R., Ligrani, P. M., Moon, H. K., and Glezer, B., "Heat Transfer and Flow Phenomena in a Swirl Chamber Simulating Turbine Blade Internal Cooling," American Society of Mechanical Engineers, ASME Paper 98-GT-466, June 1998.

[10]Ekkad, S. V., Pamula, G., and Acharya, S., "Influence of Cross-Flow Induced Swirl and Impingement on Heat Transfer in an Internal Coolant Passage of a Turbine Airfoil," *Journal of Heat Transfer*, Vol. 122, No. 3, 2000, pp. 587–597.

[11]Pamula, G., Ekkad, S. V., and Acharya, S., "Influence of Cross-Flow Induced Swirl and Impingement on Heat Transfer in a Two-Pass Channel Connected by Two Rows of Holes," *Journal of Turbomachinery*, Vol. 123, No. 2, 2001, pp. 281–287.

[12]Ekkad, S. V., and Han, J. C., "Local Heat Transfer Distributions Near a Sharp 180-deg Turn of a Two-Pass Square Channel Using a Transient Liquid Crystal Image Technique," *Journal of Flow Visualization and Image Processing*, Vol. 2, No. 3, 1995, pp. 287–298.

[13]Kline, S. J., and McClintock, F. A., "Describing Uncertainties in Single Sample Experiments," *Mechanical Engineering*, Vol. 75, No. 1, 1953, pp. 3–8.